Plasticity in carbon nanotubes: Cooperative conservative dislocation motion

Shuo Chen,[1] Elif Ertekin,[2] and D. C. Chrzan[1,*]
[1]*Department of Materials Science and Engineering, University of California, Berkeley, California 94720, USA*
[2]*Berkeley Nanoscience and Nanoengineering Institute, University of California, Berkeley, California 94720, USA*
(Received 10 December 2009; revised manuscript received 22 February 2010; published 6 April 2010)

Monte Carlo simulations are used to study dislocation glide mediated plasticity in carbon nanostructures. A detailed analysis of the simulations leads to identification of a type of defect, a dislocation screened by multiple dislocation dipoles, as the mediator of plastic deformation. The defects appear under high stress conditions. The appearance of these defects is rationalized in terms of the competition between dislocation core energy and the buckling inherent to dislocation motion within an essentially two-dimensional membrane. These defects thus represent a deformation mechanism that is uniquely found in nominally two-dimensional nanostructures. The influence of these defects on the predicted mechanical properties of carbon nanostructures is discussed.

DOI: 10.1103/PhysRevB.81.155417 PACS number(s): 62.25.−g, 61.46.−w

I. INTRODUCTION

Recent experiments into the nature of deformation and plasticity in graphene and carbon nanotubes (CNTs) suggest that the mechanical properties of two-dimensional systems are complex and unique in their own right. The intrinsic strength of these carbon-based systems is predicted to exceed that of any known material,[1] an expectation that is quantitatively supported by reported experimental measurements.[1,2] Images of topological defects in graphene and single-walled carbon nanotubes (SWNTs) have been directly obtained via high resolution transmission electron microscopy,[3] indicating that defects accumulate near kinks in the plastic deformation of the tube.[4] Experimental observations of the intrinsic ripples in graphene[5] and computational explanations thereof[6] indicate that buckling and bending play an active role in the deformation. We present here theoretical and computational evidence for a novel deformation mechanism in CNTs and possibly other sp^2 carbon systems: a stress-dependent cooperative motion of dislocations that gives rise to plasticity. This deformation mechanism exists alongside more conventional dislocation glide and arises from a complex and unique interplay between buckling, plasticity, and intrinsic defect core energies which can only occur in two-dimensional systems.

Graphene, fullerenes, CNTs, and other sp^2 carbon systems can be thought of as two-dimensional manifolds that are free to deform (bend, stretch, buckle, etc.) in the three-dimensional space in which they are embedded. The plastic deformation in sp^2 carbon systems is proving to be a very interesting phenomenon. Although direct experimental investigations into the nature of the deformation of carbon membranes have only recently become accessible, the existence of defects analogous to dislocations in conventional three-dimensional materials were previously predicted and explored computationally.[7–12] Experimental efforts[13–16] have also been undertaken to elucidate how topological (e.g., Stone-Wales) defects and their motion enable plastic deformation in these systems. For instance, CNTs have been shown to undergo elongations of over 280% at high temperature under tensile loads.[13] This elongation is accompanied by a reduction in nanotube diameter and the movement of kinks along the nanotube axis, indicating a defect-mediated mechanism of plastic deformation operational at the nanoscale. Indeed, it has long been appreciated that understanding stability, deformation, and plasticity in graphene-based systems is critical for exploiting their unique properties in real world applications.

Developing theories of plasticity in CNTs and other sp^2 carbon systems is a nontrivial endeavor. The fact that one must model large volumes of material limits progress. Even more limiting, however, is the fact that plastic deformation takes place on time scales much longer than can typically be addressed within direct atomic scale molecular dynamics (MD) methods.[17–19] In this paper, we develop a Monte Carlo sampling framework that can efficiently sample the phase space consisting of all possible C-C bond rotations in an sp^2 carbon network. Our approach discovers a novel topological defect pattern that is intrinsically different from other well documented ones, for example, vacancies,[3,20] glide,[21] brittle fracture,[21] sublimation of carbon dimers,[10,11] carbon ad dimers,[22] etc. This pattern emerges as an array of closely packed edge dislocations with alternating signs and is generally favored in tubes with large radius and under high tensile stresses. We further investigated the energetic stability of this pattern and its competing mechanisms such as dislocation glide and brittle fracture. The temperature effects on the formation of various defect patterns and the plasticity of CNTs are studied using kinetic Monte Carlo (KMC) simulations.

II. SIMULATION METHODS

Our model relies on the following assumptions to sample the potential-energy surface (PES). First, the system maintains sp^2 bonding and a constant number of atoms and bonds, i.e., N carbon atoms and $3N/2$ bonds (when periodic boundary conditions are imposed). Second, generation of four sided rings and enneagons is prohibited. The topology of the system is used to characterize the states accessible from the current state by C-C bond rotations. That is, in each Monte Carlo step, a single bond rotation drives the system from the current state to the next. For instance, starting from a defect-free carbon membrane, the rotation of the first bond creates a Stone-Wales defect. Subsequent rotations can annihilate the

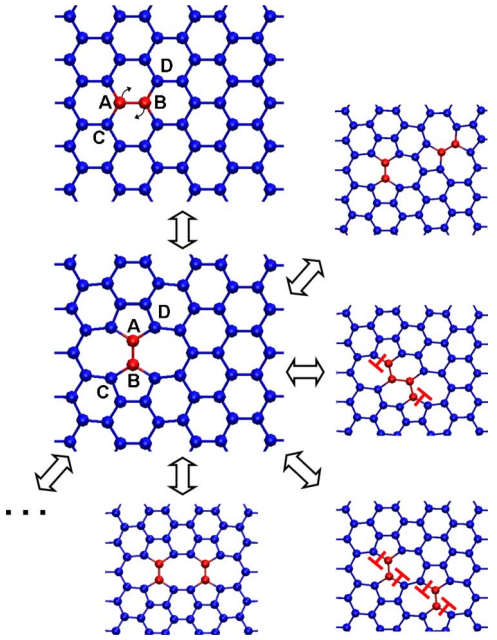

FIG. 1. (Color online) The migration of a sp^2 carbon system from one state to another by bond rotations. Each rotation involves four atoms, e.g., those labeled with A, B, C, and D. The topology of the system is changed by breaking two old bonds (e.g., AC, BD) and forming two new bonds (e.g., AD, BC).

original Stone-Wales defect, create an additional Stone-Wales defect, and create an octagon that leads to strain localization and brittle failure, or move an existing dislocation by one Burger's vector (Fig. 1). The atomic configuration of each state is optimized subject to the constraint that its bonding topology is fixed. In this way, PES local minima are sampled.

The classical reactive empirical bond order (REBO) potential[23] is employed for most of our investigations. We are primarily interested in armchair (n,n) CNTs that are believed to be ductile at low strain and high temperature.[17] Strain relaxation and creep "experiments" are implemented by applying a constant displacement per unit length or force, respectively, along the tube. Periodic boundary conditions are employed. The force normalized by the initial tube circumference is defined as the engineering stress. Geometric optimizations at each step are implemented by the fast inertial relaxation engine.[24] Forces are computed using analytical derivatives of the REBO potential. The root mean square force of the optimized structures is less than 10^{-4} eV/Å.

Within KMC transition rates from the current state to all eligible next states are defined to be $r_{ij}=\nu \exp(-E_{ij}^{\mathrm{act}}/k_BT)$ where r_{ij} is the transition rate from state i to state j, E_{ij}^{act} is the corresponding energy barrier, ν is the attempt frequency, T is the temperature, and k_B is the Boltzmann constant. The residence time on the current state and the choice of the next state are determined in the standard manner.[25] We consider two formulations. In the first, rates are determined entirely by initial and final state energies.

Unfortunately, PESs predicted by the classical REBO potential[23] are not smooth enough to have well defined Hessian Matrices at every point. The nonanalytic behavior frustrates saddle-point identification methods. To illustrate this point, the PES of creating one Stone-Wales defect within a buckyball, C_{60}, is constructed along two chosen reaction coordinates[26] while relaxing all other degrees of freedom [Fig. 2(a)]. The REBO potential leads to a PES with cusps wherever two sheets of the energy surface characterized by differing bonding topologies meet. These cusps are probably due to the bond breaking and forming during the defect nucleation and the fact that the REBO potential computes the total energy as the sum of all bond energies.

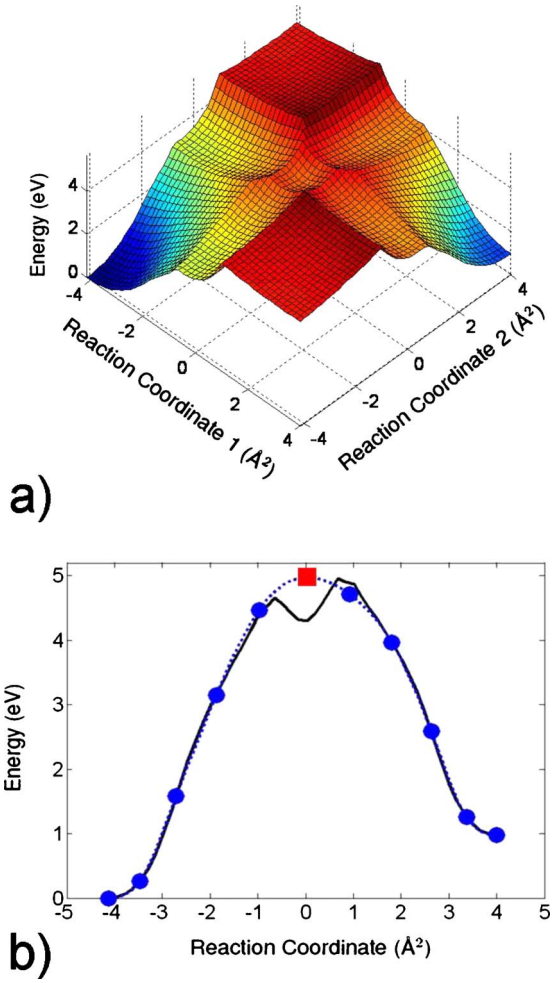

FIG. 2. (Color online) The two-dimensional (2D) PES of creating a Stone-Wales defect in C_{60} computed by the classical REBO potential (a) and the energy profile along the pseudoreaction coordinate (b) where the maximum point (the red square) is identified through natural splines (the dotted blue line) based on 10 sampled points (the blue dots). For comparison, it also shows in (b) the projection (the solid black line) of 2D PES in (a).

Therefore, as an alternative, we use an *ad hoc* pseudoreaction coordinate method to estimate energy barriers. Since each bond rotation only affects the bonding of four atoms,[26] e.g., atoms A, B, C, and D in Fig. 1, we define $\mathbf{AB}\cdot\mathbf{CD}$ as a pseudoreaction coordinate, where $\mathbf{AB}$ represents a vector connecting atom A to atom B, etc. Several constrained optimizations along a path varying the reaction coordinate are executed to locate the transition state between the initial and final states. Several points between the initial

and final configuration are sampled. At each point, **AB**·**CD** is fixed to some value and the total energy is obtained through a constrained structural optimization. The peak value of the energy path along the reaction coordinate is estimated by the choosing the maximum of a natural cubic spline passing through the sampled points.

Figure 2(b) shows an example of the energy path in the case of C_{60}. For each saddle point, we sample 10 points along the pseudoreaction coordinate. The configurations are chosen near the initial and final states. The bond in question is rotated in 0.171 rad increments for five increments from each of the end points. The peak value is identified at 5.0 eV using a natural spline interpolation, in comparison with 6.2 eV using an *ab initio* approach.[26] Figure 2(b) shows a comparison between the saddle point determined in this fashion and the PES predicted by the REBO potentials.

More generally, the approach produces a reasonable description of the energy surface. In load-free (6,6), (5,5), and (4,4) tubes, the activation energy barrier of a single Stone-Wales defect is, respectively: 9.4, 9.1, and 8.9 eV in *ab initio*[27] and 8.7, 8.5, and 8.1 eV in our calculations; in the (5,5) tube, the activation energy of the same defect at 0.06, 0.12, and 0.15 strain is, respectively: 6.5, 3.9, and 3.0 eV in *ab initio*[27] and 7.1, 4.7, and 3.1 eV in our calculations. Our approach thus yields satisfactory trends.

A typical KMC step involves a large number of atomic scale relaxations. First, each bond is identified. The bond rotation is applied, and the atomic scale structure determined along with the change in energy. In the case that computed energy barriers are incorporated into the calculation, the reaction coordinate method described above is employed. For N atoms, the system contains $3N/2$ bonds and there are two possible rotations per bond for a total of $3N$ minimizations and saddle-point identifications per KMC step. The approach is general and can incorporate PESs computed using empirical and first-principles approaches.

III. RESULTS AND DISCUSSION

As a first step, we consider a simple relaxation model in which transition rates are determined solely by the differences between initial and final energies and the process that is most rapid is always selected. These simulations are economical and enable the identification of candidate deformation mechanism. A (10,10) CNT 47.073 Å long composed of 2760 atoms and including 4140 bonds is modeled. Periodic boundary conditions are employed. Two constant engineering stress "experiments" are carried out by initially loading the tube with a fixed engineering stress of 1.105 eV/Å^2 (initial strain of ~7.8%) and a fixed engineering stress of 1.635 eV/Å^2 (initial strain of ~13.0%), respectively. The results are summarized in Figs. 3–6.

At low stress, as shown in Fig. 3, after the initial plastic event of creating a simple edge dislocation dipole separated by three burgers vectors, subsequent deformation steps simply separate the dipole. This process is equivalent to dislocation glide in three dimensional. One striking difference, however, is that the motion of dislocations in CNT leads to non-negligible buckling of the tube near the dislocations

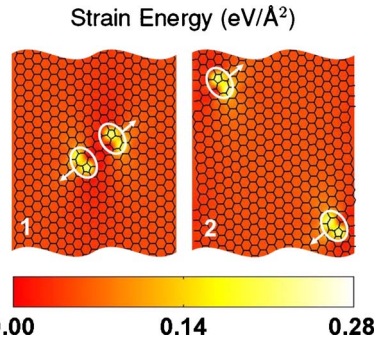

FIG. 3. (Color online) Contour plots of strain energy in (10,10) CNT with a periodic repeat length of 47.074 Å and under low axial stress (1.105 eV/Å^2). The strain energy is defined to be the local atom energy, i.e., 1/2 the bond energy of all the bonds including the considered atom, less this same bond energy in the defect- and stress-free CNT all divided by the area per atom in the unstrained CNT. The dislocations are highlighted by circles with arrows indicating the glide direction.

(Fig. 4). At high stress, as shown in Figs. 5 and 6, one sees a very different deformation pattern. The initial step is, again the creation of a simple dislocation dipole. However, instead of the dislocation gliding as at low stress, subsequent steps lead to the formation of a chain of dislocation dipoles with no net Burgers vector. Eventually, the dipole chain breaks, yielding two edge dislocations of opposite sign, each screened by an array of dislocation dipoles. The subsequent steps either lengthen these arrays by the creation of an additional dipole immediately in front of the dislocation array or shorten them by the annihilation of the trailing dipole. In this way, the two dislocation arrays glide away from each other along the slip plane in a cooperative manner, which resembles the motion of a caterpillar or worm. This detailed process is sketched in Fig. 7 and we henceforth refer to the dislocation screened by dipoles as dislocation "worms."

The appearance of worms at high stress is, at first, puzzling. Within linear elasticity theory, the worms accommodate the same level of plastic strain per step as an isolated dislocation. But in contrast, they have a larger number of dislocation cores, and one expects a larger net dislocation core energy. This dislocation core energy increase must be

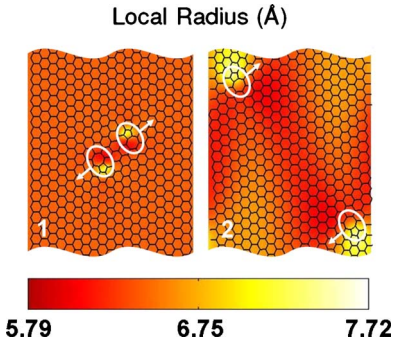

FIG. 4. (Color online) Contour plots of local tube radius corresponding to Fig. 3. It is observed that carbon nanotubes are buckled significantly near the two gliding dislocations: near the dislocations, the tube radius varies by nearly 2 Å.

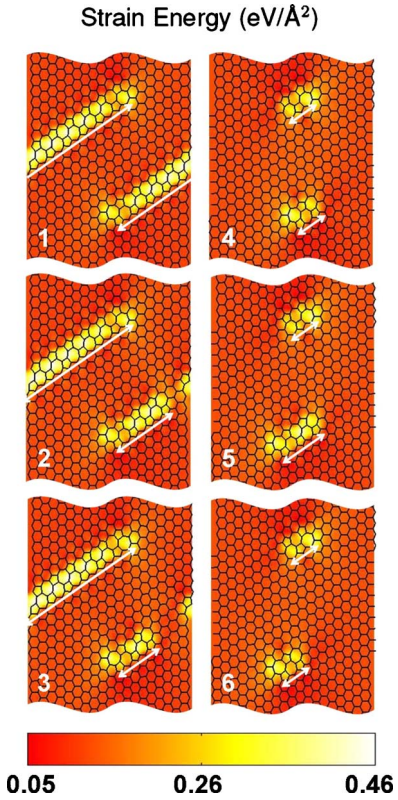

FIG. 5. (Color online) Contour plots of strain energy in (10,10) CNTs with a periodic repeat length of 47.074 Å and under high axial stress (1.635 eV/Å^2). The strain energy is defined to be the local atom energy, i.e., 1/2 the bond energy of all the bonds including the considered atom, less this same bond energy in the defect- and stress-free CNT all divided by the area per atom in the unstrained CNT. The dislocation dipole chains/worms are highlighted by double arrows. Image 1–3 show the breaking of a long dislocation chain from image 3 to image 4, two short dislocation chains are formed by annihilating several dislocation dipoles. Images 5 and 6 depict the wormlike motion of one chain.

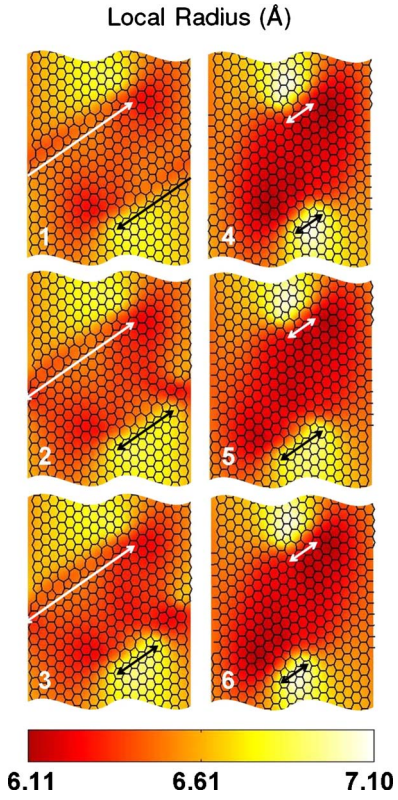

FIG. 6. (Color online) Contour plots of local tube radius corresponding to Fig. 5. Near the worms, the tube radius varies by approximately 1 Å. A comparison between these plots and those in Fig. 4 reveals that isolated dislocations introduce more buckling than dislocation worms.

balanced by another contribution to the energy.

Examination of two relaxed atomic scale configurations with equivalent plastic strain reveals the source of this additional energy: given equal plastic strain, dislocation glide is associated with a greater level of buckling within the CNT than an array of dislocation dipoles. Isolated defects generated through glide have long-ranged stress fields and consequently high local strain energies (Fig. 3). These strain energies can be relieved by buckling that introduces a curvature change in the carbon membrane near the defects at the cost of shortening the tube length and yielding less macroscopic strain. On the other hand, dislocation worms produce less strain energy than isolated dislocations because the elastic fields of closely packed dislocations are able to effectively screen each other (Fig. 5). In this case, less buckling is required to relax strain energies and thus the CNT is shortened less, but the total dislocation core energy increases. At lower stresses, the reduced macroscopic strain is not as costly as the introduction of more dislocation core energies and glide ensues. At higher stresses, screening dipoles increase the core energy, but enable larger macroscopic strains with each step.

Since the buckling energy is dependent on the radius of the CNT, it is expected that the worm length is dependent on both the applied stress and the tube radius. In addition, even when screened, the dislocations interact over long ranges. Hence the worm length should also vary as a function of local stresses, the boundary conditions (e.g., the imposed periodicity), the total plastic strain, etc. To demonstrate this dependence, we construct a plastic deformation map (Fig. 8) wherein we identify the number of dislocation dipoles formed during nucleation of individual worms under constant engineering stress conditions with periodic boundary conditions.[28] In addition, Fig. 8 identifies regions of the map in which the nanotube simply fails in a brittle fashion (energetically) and shows the yield strength of the armchair CNTs, here defined as the stress for which the formation energy of a Stone-Wales defect is equal to zero.

Several trends emerge. First, larger radii nanotubes lead to a longer chain of dislocation dipoles for a given applied stress. Second, tubes with larger radii display a transition between simple dislocation glide and worm mediated glide at a finite applied stress. Such transitions might be observable using modern microscopy techniques. Third, in the limit of zero mean curvature, i.e., infinite large radius, the CNT essentially becomes graphene with plasticity, according to the map, dominated by dislocation worms.

We have also conducted total energy electronic structure calculations of various defect configurations in graphene and

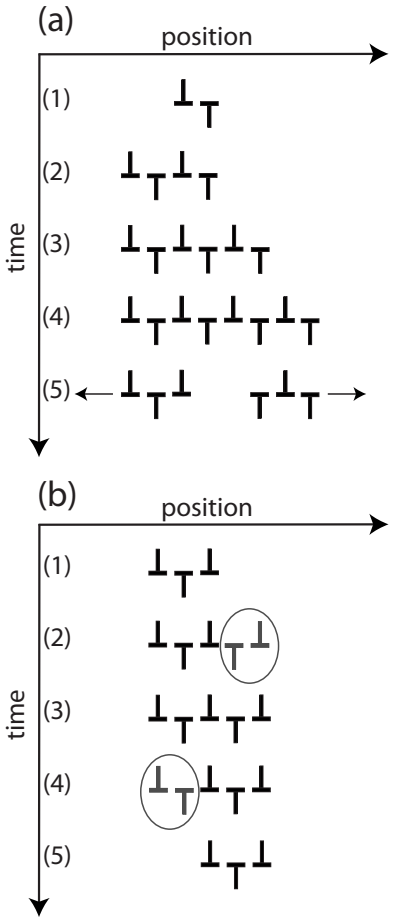

FIG. 7. (a) An illustration of the nucleation of two worms containing (nominally) three dislocations. At time step (1), a dipole is nucleated. At time (2), a second dipole adjacent to the first is nucleated. Time (3) sees the nucleation of a third dipole pair, and time (4) the fourth. At time (5), the central dipole annihilates leaving two worms of nominal length three moving the directions shown. This nucleation event would be assigned to region 4 in Fig. 8, because the worm forming structure contains four dipoles. (b) An illustration of the motion of the worm on the right at time (5) in part (a). This worm contains three to five dislocations. At time (1), the worm is in it shortest state. At time (2), the worm begins nucleating a forward dislocation pair (gray, circled). By time (3), the pair is completely formed, and the worm in its longest configuration. At time (4), the trailing dislocation pair begins annihilating (gray, circled). At time (5), the rearward pair has completely annihilated, and the worm is again in its shortest state. The net result is the advancement of the worm by a distance equal to twice the length of the Burgers vector.

carbon nanotubes in order to ensure that the patterns emerging from the REBO description persist within more accurate computational methods. The total energy electronic structure calculations reported here are conducted within density functional theory (DFT),[29,30] employ pseudopotentials[31] and invoke the local density approximation to the exchange correlation energy. Single-particle states are expanded via a plane-wave basis set. The calculated lattice constants and bulk moduli are in good agreement with experimental measurements and other theoretical results, and for each calculation we have ensured convergence with respect to both the

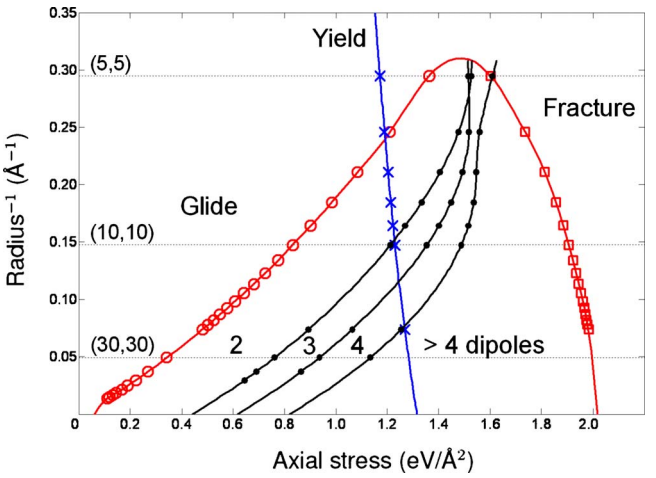

FIG. 8. (Color online) The map of plastic deformation mechanisms controlled by tube radius and axial stress for 85.2 Å long armchair CNTs under constant engineering stress conditions using formation energies of the defects. Symbols represent actual calculations and lines are guides for the eye. In the left region (low stress), dislocation glide is energetically preferred. In middle region, worms are produced from arrays of dislocation dipoles. The number indicates the number of dipoles introduced before it is favorable for the chain to break into two worms. In the right region, CNT's evolve according to the fracture pattern and fail. The yield stress as a function of tube radius is also plotted for reference.

k-point mesh and the plane wave cutoff. Tables I and II summarize the results obtained for a (7,7) carbon nanotube (192 atom supercell) and a 180 atom graphene supercell, respectively.

A (7,7) carbon nanotube represented by a 196 atom supercell under tensile loads of 0%, 3.6%, and 11.0% strain was initially considered. In this system, we find that again, worms are favored over glide at high strains where buckling is suppressed (e.g., at 3.6% and 11.0% strain), while as expected, in the unstrained nanotube where buckling is favorable, the formation energy for the isolated dislocation (glide) is lower than that of the worm. By comparison, for the same system now described by REBO, glide is favored for the unstrained and 3.6% strained system, while worms are favored at 11.6% strain. Thus, the trends obtained by the two methods are similar, although in DFT the transition from

TABLE I. Defect formation energies in (7,7) carbon nanotube computed via DFT.

(7,7) Carbon nanotubes			
Strain e_{zz}	0%	3.6%	11.0%
Defect formation energies from DFT (eV)			
SW	4.05	1.68	−3.48
Glide	6.89	3.03	−6.25
Worm	7.72	2.80	−7.60
Glide vs Worm energy (eV)			
$E_g - E_w$ (DFT)	−0.83	0.23	1.35
$E_g - E_w$ (REBO)	−2.54	−1.04	0.42

TABLE II. Defect formation energies in Graphene computed via DFT.

Graphene sheet			
Strain e_{zz}	0%	1.9%	8.4%
Defect formation energies from DFT (eV)			
SW	4.88	3.87	−0.78
Glide	10.09	8.78	0.22
Worm	8.99	7.55	−1.81
Glide vs Worm energy (eV)			
$E_g - E_w$ (DFT)	1.10	1.23	2.03
$E_g - E_w$ (REBO)	−0.13	0.20	1.15

glide- to worm- mediated deformation takes place at even smaller strains. We also compared the same defect formation energies in a 180 atom graphene sheet at strains of 0%, 1.9%, and 8.4%. In this system, we find that DFT always favors worms over glide for all strains, while REBO does in fact favor glide at 0% strain (although only by 0.13 eV) and then quickly transitions into worm-mediated deformation before 1.9%. Thus, the DFT calculations demonstrate that qualitatively, the patterns described by the REBO description persist, although it appears that DFT favors worm formation over isolated dislocations even more strongly than the empirical potentials (i.e., the transition line between glide and worms in Fig. 8 is pushed toward the left).

Finally, we explored the effects of introducing temperature and computed energy barriers for each bond rotation.

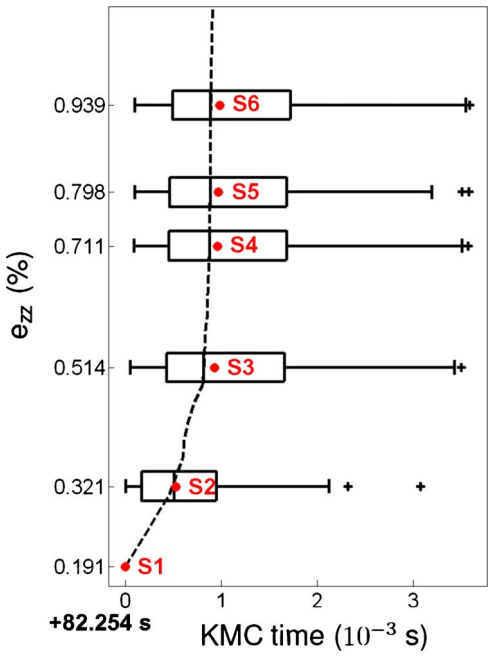

FIG. 9. (Color online) The engineering strain versus time curve (dash line) at 2000 K after the formation of an initial Stone-Wales defect. The KMC time data from 40 runs of the same KMC simulation with different random seeds are summarized in box plots. Each box plot depicts the data through the five number summaries, i.e., the smallest observation, lower quantile, median, upper quantile, and largest observation, plus possible outliers.

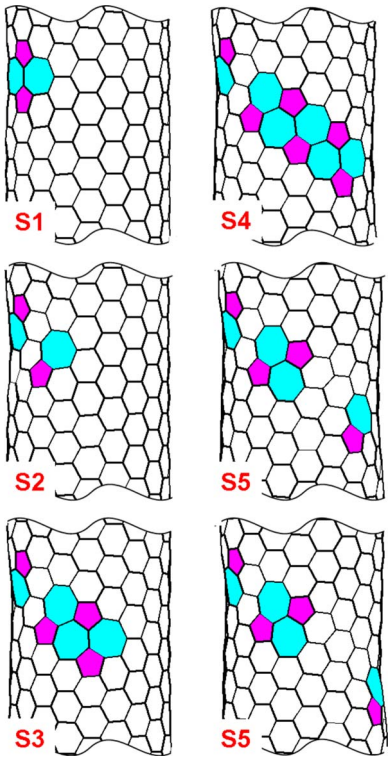

FIG. 10. (Color online) Typical snapshots of CNT at several strains in the KMC simulation where image S1–S6 correspond to point S1–S6 in Fig. 9. Image S1 shows the nucleation a single SW defect, i.e., an edge dislocation dipole which glides by one step in image S2. In image S3, S4, and S5, a chain of five dislocations is formed and then breaks in the middle, leaving a single dislocation in one end. This dislocation then glides in image S6.

KMC simulations are used to model a constant engineering stress experiment with a (10,10) armchair CNT (800 atoms and 1200 bonds) loaded with an engineering stress of 1.0 eV/Å^2 (~7.0% initial elastic strain) along the tube axis. The temperature is fixed at 2000 K, below the sublimation temperature of CNT (~2500 K).

Figures 9 and 10 summarize simulation outcomes of 40 runs of the same KMC simulation with different random seeds. At each selected strain, the KMC time data are represented by a box plot[32] where the box shows the 0.25 quartile, the sample median and the 0.75 quartile, and the whiskers indicate the sample minimum and the sample maximum, and plus symbols suggest possible outliers. The initial Stone-Wales defect is nucleated from the defect-free material, taking 81.5 s on average, and then the tube elongates rapidly, in accordance with previous results.[33] Along the strain-time curve, some snapshots of the system extracted from a typical KMC run suggest that the plasticity is achieved by a combination of different mechanisms, e.g., dislocation glide, defect nucleation, defect annihilation, etc. We note that the formation of dislocation chains persists, even when energy barriers are included, indicating that this plasticity mechanism should in fact occur alongside other mechanisms in experiment. Finally, the times reported for the simulations are based on the assumption that $\nu = 10^{13}$ sec^{-1}. We believe this to be a reasonable order of magnitude estimate for the attempt fre-

quency for bond rotation, but note that further study is warranted.

It is also noted that the strain increment from one snapshot to the next is not uniform, although in all cases, the origin is the movement of an edge dislocation by one Burgers vector. If $\Delta e(X,Y)$ is used to indicate the strain increment from the snapshot X to Y, then qualitatively we have $\Delta e(\mathrm{S2},\mathrm{S3}) \approx \Delta e(\mathrm{S3},\mathrm{S4}) > \Delta e(\mathrm{S1},\mathrm{S2}) \approx \Delta e(\mathrm{S5},\mathrm{S6}) > \Delta e(\mathrm{S4},\mathrm{S5})$. Interestingly, the process S2,S3 or S3,S4 increases a dislocation chain; S1,S2 or S5,S6 makes a dislocation glide; S4,S5 annihilates a defect. Thus within the atomic scale calculations, the increment of strain associated with dislocation motion is not fixed completely by the Burgers vector of the dislocation, but is also influenced by the degree of buckling.

If plasticity is mediated by worms, one might expect this to have an impact on measured properties. For example, the number of slip planes intersected by dislocation cores comprising a single worm is certainly larger than that of isolated dislocations. If dislocations on differing slip planes interact with contact forces, worms will increase the extent of this interaction substantially, possibly yielding an increase in hardening rate.

IV. CONCLUSION

In summary, we have developed a phase-space sampling technique to study topological defect dynamics in CNTs. We have discovered a defect pattern, dislocation worms that are energetically favored in CNTs with larger radii. In comparison with dislocation glide, dislocation worms lead to less buckling of the carbon membrane and hence allow more effective plastic elongation along the axial direction. KMC simulations enable modeling of more realistic time scales by explicitly reflecting computed energy barriers and are used to explore the strain-time relationship in strain relaxation experiments. Nucleation of the first Stone-Wales defect is the strain rate controlling step. Subsequent steps produce various defect patterns including dislocation glide, dipole nucleation, and annihilation.

ACKNOWLEDGMENTS

This work was supported by the National Science Foundation within the Center of Integrated Nanomechanical systems under Grant No. EEC-0425914. E.E. acknowledges funding by the Focus Center Research Program on Materials, structures, and Devices (FCRP/MSD). This research used computational resources of the National Energy Research Scientific Computer Center, which is supported by the Office of Science of the U.S. Department of Energy under Contract No. DE-AC02-05CH11231.

*Corresponding author; dcchrzan@berkeley.edu

[1] B. Peng, M. Locascio, P. Zapol, S. Li, S. L. Mielke, G. C. Schatz, and H. D. Espinosa, Nat. Nanotechnol. **3**, 626 (2008).
[2] C. Lee, X. Wei, J. W. Kysar, and J. Hone, Science **321**, 385 (2008).
[3] A. Hashimoto, K. Suenaga, A. Gloter, K. Urita, and S. Iijima, Nature **430**, 870 (2004).
[4] K. Suenaga, H. Wakabayashi, M. Koshino, Y. Sato, K. Urita, and S. Iijima, Nat. Nanotechnol. **2**, 358 (2007).
[5] J. C. Meyer, A. K. Geim, M. I. Katsnelson, K. S. Novoselov, T. J. Booth, and S. Roth, Nature **446**, 60 (2007).
[6] A. Fasolino, J. H. Los, and M. I. Katsnelson, Nature Mater. **6**, 858 (2007).
[7] Z. Li, P. Dharap, P. Sharma, S. Nagarajaiah, and B. Yakobson, J. Appl. Phys. **97**, 074303 (2005).
[8] E. Ertekin, M. S. Daw, and D. C. Chrzan, Philos. Mag. Lett. **88**, 159 (2008).
[9] E. Ertekin, D. C. Chrzan, and M. S. Daw, Phys. Rev. B **79**, 155421 (2009).
[10] F. Ding, K. Jiao, M. Wu, and B. I. Yakobson, Phys. Rev. Lett. **98**, 075503 (2007).
[11] F. Ding, K. Jiao, Y. Lin, and B. I. Yakobson, Nano Lett. **7**, 681 (2007).
[12] Q. Zhao, M. Buongiorno Nardelli, and J. Bernholc, Phys. Rev. B **65**, 144105 (2002).
[13] J. Huang, S. Chen, Z. Wang, K. Kempa, Y. Wang, S. Jo, G. Chen, M. Dresselhaus, and Z. Ren, Nature **439**, 281 (2006).
[14] J. Y. Huang, S. Chen, Z. F. Ren, Z. Q. Wang, D. Z. Wang, M. Vaziri, Z. Suo, G. Chen, and M. S. Dresselhaus, Phys. Rev. Lett. **97**, 075501 (2006).
[15] J. Y. Huang, S. Chen, Z. F. Ren, Z. Wang, K. Kempa, M. J. Naughton, G. Chen, and M. S. Dresselhaus, Phys. Rev. Lett. **98**, 185501 (2007).
[16] J. Y. Huang, F. Ding, and B. I. Yakobson, Phys. Rev. Lett. **100**, 035503 (2008).
[17] M. Buongiorno Nardelli, B. I. Yakobson, and J. Bernholc, Phys. Rev. Lett. **81**, 4656 (1998).
[18] M. Buongiorno Nardelli, B. I. Yakobson, and J. Bernholc, Phys. Rev. B **57**, R4277 (1998).
[19] C. Tang, W. Guo, and C. Chen, Phys. Rev. B **79**, 155436 (2009).
[20] A. T. Lee, Y.-J. Kang, K. J. Chang, and I.-H. Lee, Phys. Rev. B **79**, 174105 (2009).
[21] B. Yakobson, Appl. Phys. Lett. **72**, 918 (1998).
[22] M. Sternberg, L. A. Curtiss, D. M. Gruen, G. Kedziora, D. A. Horner, P. C. Redfern, and P. Zapol, Phys. Rev. Lett. **96**, 075506 (2006).
[23] D. Brenner, O. Shenderova, J. Harrison, S. Stuart, B. Ni, and S. Sinnott, J. Phys.: Condens. Matter **14**, 783 (2002).
[24] E. Bitzek, P. Koskinen, F. Gahler, M. Moseler, and P. Gumbsch, Phys. Rev. Lett. **97**, 170201 (2006).
[25] A. Bortz, M. H. Kalos, and J. L. Lebowitz, J. Comput. Phys. **17**, 10 (1975).
[26] B. Eggen, M. Heggie, G. Jungnickel, C. Latham, R. Jones, and P. Briddon, Science **272**, 87 (1996).
[27] T. Dumitrica and B. Yakobson, Appl. Phys. Lett. **84**, 2775 (2004).
[28] To save computational time, we consider only one length tube

with periodic boundary conditions imposed. Spot calculations using tubes of varying length reveal similar phenomenology, but differing transition stresses for mechanisms. This is consistent with the long-ranged nature of the defect interactions within these nanostructures.

[29] G. Kresse and J. Fürthmuller, Phys. Rev. B **54**, 11169 (1996).
[30] G. Kresse and J. Fürthmuller, Comput. Mater. Sci. **6**, 15 (1996).
[31] D. Vanderbilt, Phys. Rev. B **32**, 8412 (1985).
[32] J. W. Tukey, *Exploratory Data Analysis* (Addison-Wesley, Reading, MA, 1997).
[33] H. Mori, S. Ogata, J. Li, S. Akita, and Y. Nakayama, Phys. Rev. B **74**, 165418 (2006).